Wnt7a stimulates myogenic stem cell motility and engraftment resulting in improved muscle strength

C. Florian Bentzinger,[1,2] Julia von Maltzahn,[1,2] Nicolas A. Dumont,[1,2] Danny A. Stark,[3] Yu Xin Wang,[1,2] Kevin Nhan,[1,2] Jérôme Frenette,[5] DDW Cornelison,[3,4] and Michael A. Rudnicki[1,2]

[1]Regenerative Medicine Program, Ottawa Hospital Research Institute, Ottawa, ON K1H 8L6, Canada
[2]Faculty of Medicine, Department of Cellular and Molecular Medicine, University of Ottawa, Ottawa, ON K1H 8M5, Canada
[3]Division of Biological Sciences and [4]Christopher S. Bond Life Sciences Center, University of Missouri, Columbia, MO 65211
[5]Faculty of Medicine, Department of Rehabilitation, Laval University, Quebec City, QC G1V 4G2, Canada

Wnt7a/Fzd7 signaling stimulates skeletal muscle growth and repair by inducing the symmetric expansion of satellite stem cells through the planar cell polarity pathway and by activating the Akt/mTOR growth pathway in muscle fibers. Here we describe a third level of activity where Wnt7a/Fzd7 increases the polarity and directional migration of mouse satellite cells and human myogenic progenitors through activation of Dvl2 and the small GTPase Rac1. Importantly, these effects can be exploited to potentiate the outcome of myogenic cell transplantation into dystrophic muscles. We observed that a short Wnt7a treatment markedly stimulated tissue dispersal and engraftment, leading to significantly improved muscle function. Moreover, myofibers at distal sites that fused with Wnt7a-treated cells were hypertrophic, suggesting that the transplanted cells deliver activated Wnt7a/Fzd7 signaling complexes to recipient myofibers. Taken together, we describe a viable and effective ex vivo cell modulation process that profoundly enhances the efficacy of stem cell therapy for skeletal muscle.

Introduction

Satellite cells reside closely juxtaposed to myofibers beneath the basal lamina and are responsible for the growth and repair of skeletal muscle (Yin et al., 2013b). The paired-box transcription factor Pax7 is expressed in all satellite cells and plays an essential role in regulating the expansion and differentiation of satellite cells during both neonatal and adult myogenesis (Seale et al., 2000; Relaix et al., 2006; von Maltzahn et al., 2013a). Pax7 functions as a nodal factor establishing the myogenic identity and allowing proliferation while preventing differentiation (Soleimani et al., 2012).

Satellite cells are a heterogeneous population composed of primarily committed progenitors and a small subpopulation of self-renewing satellite stem cells (Kuang et al., 2007). Lineage tracing using *Myf5-Cre* and *R26R-YFP* reporter alleles indicates that ~10% of these satellite cells have never expressed the myogenic regulatory factor Myf5. These Pax7$^+$/YFP$^-$ satellite stem cells extensively contribute to the satellite cell pool after transplantation into muscle. By contrast, Pax7$^+$/YFP$^+$ satellite myogenic cells, which have expressed Myf5-Cre, are committed to undergo differentiation and do not contribute to the satellite cell pool. Upon activation, satellite stem cells can either undergo a symmetric planar cell division, or alternatively undergo an asymmetric apical–basal cell division to give rise to a satellite myogenic cell (Kuang et al., 2007). Therefore, satellite cells are a heterogeneous population composed of a small fraction of satellite stem cells and a large number of committed satellite myogenic cells (Kuang et al., 2008).

Our recent work has shown that the size of the satellite stem cell pool is critically controlled by the planar cell polarity signaling pathway. Satellite stem cells express high levels of Frizzled 7 (Fzd7) and Vangl2 (Le Grand et al., 2009). Wnt7a stimulation of Fzd7 leads to cellular polarization and selectively increases symmetric stem cell expansion. Treatment of regenerating muscles with Wnt7a accelerates muscle repair by boosting the number of satellite stem cells and ultimately the overall satellite cell pool (Le Grand et al., 2009; Bentzinger et al., 2013b).

C.F. Bentzinger and J. von Maltzahn contributed equally to this paper.

Correspondence to Michael A. Rudnicki: mrudnicki@ohri.ca

J. von Maltzahn's present address is Fritz Lipmann Institute for Age Research, 07745 Jena, Germany.

Abbreviations used in this paper: Dvl, Disheveled; Fzd, Frizzled.

© 2014 Bentzinger et al. This article is distributed under the terms of an Attribution–Noncommercial–Share Alike–No Mirror Sites license for the first six months after the publication date (see http://www.rupress.org/terms). After six months it is available under a Creative Commons License (Attribution–Noncommercial–Share Alike 3.0 Unported license, as described at http://creativecommons.org/licenses/by-nc-sa/3.0/).

The Rockefeller University Press $30.00
J. Cell Biol. Vol. 205 No. 1 97–111
www.jcb.org/cgi/doi/10.1083/jcb.201310035

After satellite cell activation, Fzd7 is expressed in myogenic progenitors (Le Grand et al., 2009). However, a function in this cell type has not yet been described. Fzd7 is also expressed by postmitotic muscle fibers where Wnt7a/Fzd7 signaling leads to an induction of the Akt/mTOR anabolic growth pathway, leading to increases in muscle size and strength (von Maltzahn et al., 2011, 2012). Direct injection Wnt7a into dystrophin-deficient *mdx* muscle ameliorates the dystrophic phenotype, resulting in improved force generation (von Maltzahn et al., 2012). Taken together, these experiments suggest that stimulation of muscle cells with Wnt7a has potential therapeutic applications.

Muscle tissue can be affected by a plethora of pathological conditions, most prominently by the muscular dystrophies (Rüegg and Glass, 2011). More than 30 genes have been implicated in different forms of muscular dystrophy. Muscle stem cells, or satellite cells, have the ability to correct these genetic defects by introducing their genome to the syncytial muscle fibers through fusion (Wang and Rudnicki, 2012). This capability makes satellite cells attractive candidates for stem cell therapy of muscle diseases. However, in spite of significant research efforts such therapies for skeletal muscle tissue have not yet reached the clinic (Bareja and Billin, 2013). Difficulties in obtaining sufficient donor cells, poor survival, engraftment, and dispersal of transplanted cells in muscle tissue are fundamental problems that have not yet been resolved (Bentzinger et al., 2012).

By contrast, stem cell therapy for disorders of the hematopoietic system has been practiced for decades (Jenq and van den Brink, 2010). Due to their low immunogenicity and primitiveness, hematopoietic stem cells (HSCs) obtained from umbilical cord blood have recently emerged as the preferred cell type for these treatments. However, the number of HSCs that can be isolated from a single cord is limited. Unfortunately, combining two or more cord blood–derived cell populations increases the risk of immunogenicity of the transplant. Therefore, strategies that enhance the efficiency of engraftment and reduce the required cell dose to a level that requires only one donor cord are currently being explored in clinical trials. In particular, ex vivo pharmacologic modulation that positively influences homing and survival has emerged as a method to reduce the number of HSCs required for a successful therapeutic outcome (North et al., 2007; Hoggatt et al., 2009).

Along the same lines, compounds for pharmacological improvement of muscle stem cell engraftment would be of great use for the development of cell therapies for muscle disease. Ideally, such a compound would not only enhance the efficiency of engraftment but also facilitate an even distribution of donor cells in the host tissue.

Due to the manifold positive effects of Wnt7a on cells of the muscle lineage (Le Grand et al., 2009; von Maltzahn et al., 2011, 2012), we set out to test its potential to improve the outcome of myogenic cell therapy. We demonstrate that a short ex vivo treatment of human or mouse myogenic cells with Wnt7a is sufficient to significantly enhance engraftment and tissue dispersion in dystrophic muscle. Strikingly, fusion of Wnt7a-loaded myogenic progenitors to host myofibers leads to a profound hypertrophic response and improved force generation. Taken together, we describe a unique pharmacologic means to improve the outcome of cell therapy for skeletal muscle–associated diseases.

Results

Wnt7a and Fzd7 polarize myogenic cells and stimulate directed cell migration

Cell migration is typically accompanied by cytoskeletal polarization, leading to a distinctive triangular cell shape. We found that incubation of C2C12 myoblasts with Wnt7a led to a 111% increase in the abundance of triangular polarized cells (Fig. 1 A and Fig. S1 A). We previously demonstrated that the major receptor of Wnt7a in myogenic cells is Fzd7 (Le Grand et al., 2009) and that overexpression of Fzd7 alone is sufficient to induce signaling (von Maltzahn et al., 2011; Bentzinger et al., 2013b). In agreement with these observations, we found that expression of Fzd7-YFP induced polarization by 130% (Fig. 1 A and Fig. S1 A). Treatment of Fzd7-YFP–expressing cells with Wnt7a increased cell polarization by 167%, but was not significantly different from the Wnt7a or Fzd7-YFP conditions alone.

With the YFP epitope tag on our Fzd7 construct, we were able to examine its subcellular localization. A majority of Fzd7-YFP was found in small intracellular vesicles associated with the tubulin cytoskeleton in C2C12 cells (Fig. 1 B). By contrast, no such localization could be observed for YFP alone (Fig. S1 B). In live-imaging movies, we observed that Fzd7-YFP also accumulates in the periphery of migrating cells (Fig. 1 C and Video 1), whereas YFP alone did not show such a polarized localization (Fig. 1 C and Video 2). We also observed peripheral localization of Fzd7-YFP in transfected primary mouse myoblasts (Fig. S1 C), mouse satellite cells (Fig. S1 D), and human myoblasts (Fig. S1 E). Importantly, the peripheral localization of Fzd7-YFP was not due to its transmembrane nature because an unrelated canonical Fzd, Fzd3-YFP, did not exhibit this localization (Fig. 1 D and Fig. S1 F).

Cellular polarization is indicative of increased motility (de Forges et al., 2012). Therefore, we set out to test whether Wnt7a and Fzd7 affect this characteristic in scratch assays. To exclude effects on the localization of cells arising from altered rates of proliferation, we treated the cells with mitomycin-C. Addition of Wnt7a to the culture medium increased the migration of C2C12 cells by 443% (Fig. 1, E and F). Similarly, overexpression of Fzd7-Flag resulted in a 401% increase in cell migration (Fig. 1 G).

Wnt7a treatment and Fzd7-Flag overexpression also increased cell migration by 136% and 167%, respectively, in satellite cell–derived mouse primary myoblasts (Fig. 2, A and B). The effect of Wnt7a signaling on cell migration was dependent on Fzd7 because myoblasts derived from Fzd7 knockout mice (Yu et al., 2012) showed no reaction to this factor (Fig. 2 C and Fig. S2 A). When compared with heterozygous myoblasts, Fzd7-deficient cells migrated 59% less and expression of Fzd7-Flag in Fzd7 knockout myoblasts restored migration to normal levels (Fig. 2 D). An unrelated canonical Wnt, Wnt3a, did not have significant effects on cell migration of primary mouse myoblasts (Fig. 2 E). To investigate whether the stimulation of myoblast

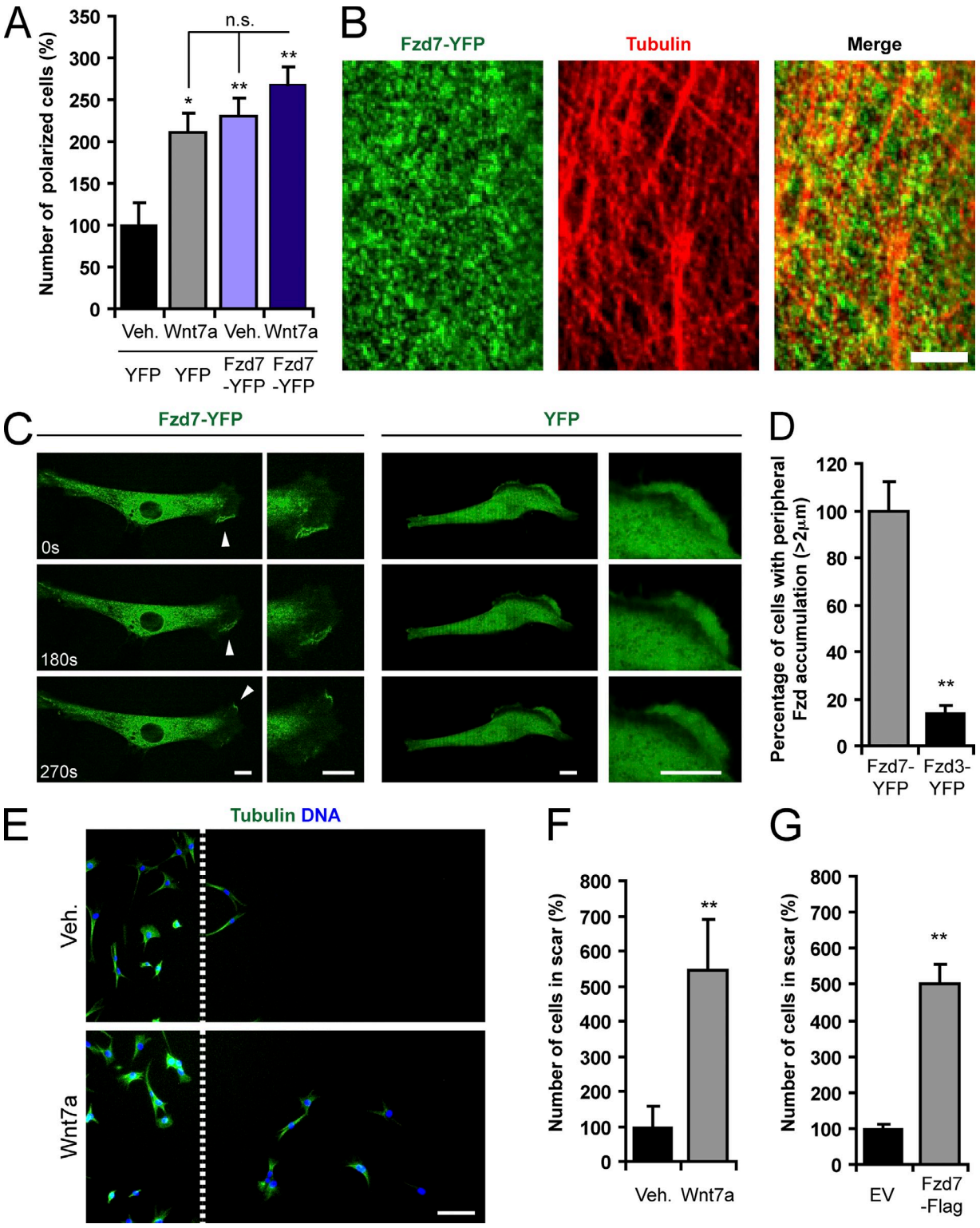

Figure 1. **Wnt7a and Fzd7 induce the polarization and migration of myogenic cells.** (A) Morphological quantification of triangular polarized C2C12 cells upon Wnt7a stimulation and Fzd7 overexpression. Vehicle (Veh.)-treated cells expressing YFP were set to 100%. Error bars represent means ± SEM; $n \geq 4$. *, $P < 0.05$; **, $P < 0.01$. n.s., no significant difference. (B) Confocal images showing the localization of Fzd7-YFP and the tubulin cytoskeleton of a C2C12 cell. Bar, 4 μm. (C) Sequences derived from live imaging of C2C12 cells that were transfected with Fzd7-YFP or YFP at the given time points. The arrowheads show peripheral Fzd7-YFP that is dynamically rearranged during cell migration. Bar, 10 μm. (D) Frequency of peripheral Fzd7-YFP accumulation in C2C12 cells when compared with Fzd3-YFP. Fzd7-YFP was set to 100%. Error bars represent means ± SEM; $n = 3$. **, $P < 0.01$. (E) Representative images from scratch assays with C2C12 cells. The dashed line represents the border of the scratch wound. Cells that were treated with Wnt7a migrate farther than vehicle-treated cells. Bar, 100 μm. (F) Quantification of C2C12 migration in scratch assays as shown in E. Wnt7a significantly increases migration compared with vehicle. Error bars represent means ± SEM; $n = 3$. **, $P < 0.01$. (G) Overexpression of Fzd7-Flag also increases the migration of C2C12 cells in scratch assays when compared with empty vector (EV). Error bars represent means ± SEM; $n = 3$. **, $P < 0.01$.

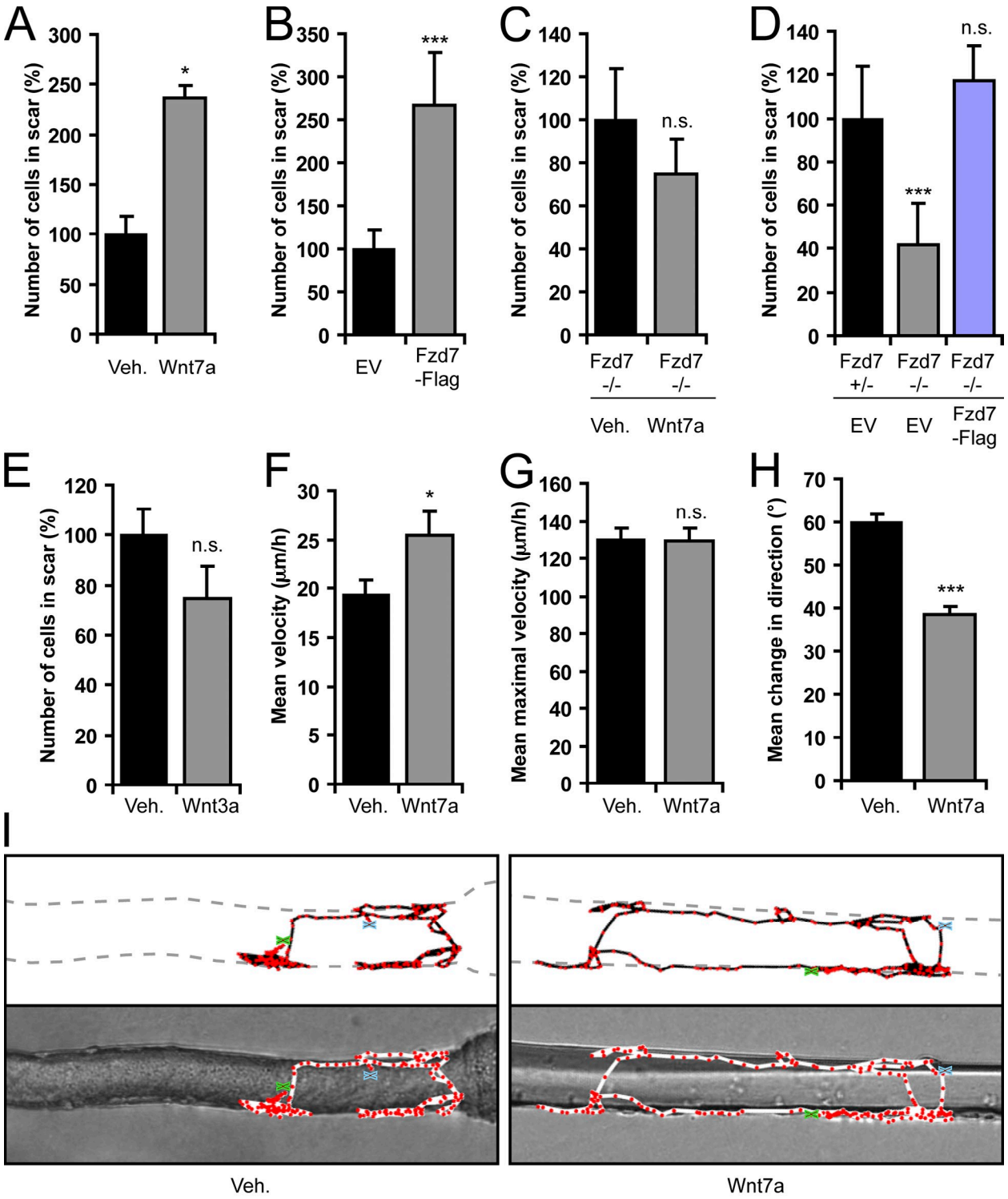

Figure 2. **Wnt7a and Fzd7 facilitate directed cell migration.** (A) Scratch migration assay with mouse primary myoblasts that were stimulated with Wnt7a or vehicle. Error bars represent means ± SEM; $n = 3$. *, $P < 0.05$. (B) Quantification of scratch assays using primary myoblasts overexpressing EV or Fzd7-Flag. Error bars represent means ± SEM; $n = 3$. ***, $P < 0.001$. (C) Primary myoblasts derived from Fzd7 knockout mice ($Fzd7^{-/-}$) do not respond to Wnt7a stimulation. Error bars represent means ± SEM; $n \geq 3$. n.s., no significant difference. (D) Scratch migration assay showing that $Fzd^{-/-}$ primary myoblasts migrate significantly less than heterozygous cells ($Fzd7^{+/-}$). Genetic Fzd7 knockout can be rescued by expression of Fzd7-Flag. Error bars represent means ± SEM; $n = 3$. ***, $P < 0.001$. (E) Quantification showing that canonical Wnt3a does not affect cell migration in scratch wound assays. Error bars represent means ± SEM; $n = 3$. (F) Mean velocity of satellite cells on single cultured myofibers as determined by live imaging. Error bars represent means ± SEM; $n \geq 27$. *, $P < 0.05$. (G) The mean maximal speed of Wnt7a-stimulated satellite cells is not significantly different from the vehicle control. Error bars represent means ± SEM; $n \geq 27$. (H) Quantification of the mean change in direction of Wnt7a-treated satellite cells. In the presence of Wnt7a the cells migrate with increased directional persistence when compared to vehicle. Error bars represent means ± SEM; $n \geq 27$. ***, $P < 0.001$. (I) Representative tracks of satellite cells on single cultured myofibers. The green "x" represents the start of imaging, and the blue "x" is the stop. Fewer changes in directional motility can be observed for the Wnt7a-treated satellite cell.

migration is dose dependent, we tested different concentrations of Wnt7a and Wnt3a for their effect on migration. Whereas increasing concentrations of Wnt7a caused a relatively linear increase in cell migration, the canonical Wnt3a had no significant effect at any concentration tested (Fig. S2 B).

To test a possible effect of Wnt7a on satellite cell migration we used a time-lapse imaging technique previously used to monitor satellite cells on single muscle myofibers (Siegel et al., 2009). These experiments revealed that Wnt7a increases the mean velocity of satellite cells by 31% when compared with vehicle (Fig. 2 F and Video 3). Interestingly, the mean maximal velocity was not statistically different between Wnt7a and vehicle (Fig. 2 G). The increase in mean velocity was therefore likely caused by the 36% higher directional persistence of Wnt7a-treated satellite cells (Fig. 2, H and I). Therefore, our results indicate that activation of Wnt7a/Fzd7 signaling markedly stimulates the motility of satellite cells and myogenic progenitors by inducing polarization and enhancing directionality of migration.

Wnt7a-induced cell migration requires Dvl2 and Rac1

Our previous work revealed a requirement of Rac1 for Wnt7a signaling in satellite cells (Bentzinger et al., 2013b). We observed that polarized peripheral Fzd7-tdTomato colocalized with GFP-Rac1 in C2C12 cells (Fig. 3 A). This suggested that the small GTPase Rac1 might also be involved in Wnt7a-mediated cell polarization and migration. In agreement with this hypothesis, overexpression of Wnt7a significantly increased the activation of Rac1 (Fig. 3 B and Fig. S3 A). Many forms of Wnt signaling require Disheveled (Dvl) proteins. At the protein level, Dvl2 is the most expressed Dvl in mouse primary myoblasts (unpublished data). siRNA SMARTpool-mediated knockdown of Dvl2 (siDvl2) from Wnt7a-stimulated cells significantly reduced the activation of Rac1 when compared with the scrambled siRNA (siSCR) control (Fig. 3 B and Fig. S3, A and B). Dvl has been suggested to serve as a scaffolding protein for downstream Wnt signaling effectors. Indeed, we observed an increased Rac1 association with Dvl2 in Wnt7a-stimulated cells (Fig. 3 C and Fig. S3 C).

As predicted by these results, siDvl2 prevented both Wnt7a- and Fzd7-Flag overexpression–mediated migration of mouse primary myoblasts in scratch assays (Fig. 3, D and E). Moreover, the expression of dominant-negative Rac1-T17N (Rac1-DN) also antagonized Wnt7a- and Fzd7-mediated migration in primary mouse myoblasts (Fig. 3, F and G). Our biochemical analysis revealed no significant activation of other small GTPases such as Cdc42 and RhoA (unpublished data). Nevertheless, both dominant-negative Cdc42-T17N (Cdc42-DN) and RhoA-T19N (RhoA-DN) were able to prevent Wnt7a-induced cell migration (Fig. S3 D). Thus, we conclude that Dvl2 and the small GTPases Rac1, Cdc42, and RhoA are essential for the induction of cell motility by Wnt7a.

Wnt7a signaling in myoblasts is strictly noncanonical

Wnt7a at a concentration of 50 ng/ml does not activate β-catenin in satellite cells, primary myoblasts (Le Grand et al., 2009), or muscle myofibers (von Maltzahn et al., 2011). Moreover, ectopic expression of Wnt7a does not induce the TOP-flash luciferase reporter (Molenaar et al., 1996) in C2C12 myoblasts (Kuroda et al., 2013). To further clarify the signaling mechanisms downstream of Wnt7a and to exclude a dose-dependent effect on β-catenin, we tested different concentrations of this factor for its ability to induce TOP-flash activity in C2C12 cells. Although the canonical Wnt3a showed a dose-dependent response (Fig. 4 A), increasing concentrations of Wnt7a had no effect on TOP-flash reporter activity (Fig. 4 B). Collectively, these data support the notion that Wnt7a signaling in all cells of the adult muscle lineage is strictly noncanonical.

Endocytosis is required for Wnt7a-induced cell migration

The activation of Rac1 by noncanonical Wnt signals has been shown to depend on clathrin-mediated endocytosis (Sato et al., 2010). Therefore, we set out to test whether Wnt7a treatment could alter the subcellular distribution of Fzd7. Indeed, Wnt7a-stimulated primary myoblasts displayed a higher abundance of large intracellular aggregates and reduced peripheral Fzd7-YFP (Fig. 4 C). In agreement with this observation, treatment with monodansylcadaverine, an inhibitor of clathrin-mediated endocytosis (Schlegel et al., 1982), prevented Wnt7a-mediated migration in scratch assays (Fig. 4 D). Importantly, we observed that myoblasts that were exposed to conditioned medium containing HA epitope-tagged Wnt7a (Wnt7a-HA) quickly endocytosed this factor. After 3 h of incubation and several subsequent washing steps, endocytosed Wnt7a-HA was detectable for ≥72 h in intracellular structures in primary myoblasts (Fig. 4 E) and C2C12 cells (Fig. S3 E). No intracellular Wnt7a-HA could be observed in *Fzd7*$^{-/-}$ myoblasts exposed to the conditioned medium (Fig. 4 E). These observations demonstrate that both Fzd7 and Wnt7a endocytosis are interdependent and require activation of noncanonical signaling in myoblasts. Moreover, the endocytosis of Wnt7a was surprisingly fast and the protein appeared to be present in intracellular stores for prolonged periods. Taken together, these observations suggest that a short exposure to Wnt7a has sustained effects on myogenic cells.

Wnt7a treatment facilitates the migration of primary myoblasts in vivo

We next set out to investigate whether loading of intracellular stores with Wnt7a would have long-lasting effects on cell migration. We exposed tdTomato-expressing primary myoblasts, derived from tamoxifen-treated *Pax7-CreER;R26R-tdTomato* mice (Yin et al., 2013a), for 3 h to Wnt7a, washed the cells, and transplanted them into the tibialis anterior muscle of immunosuppressed C57BL/6 mice (Fig. 5 A). To identify the injection site in subsequent analysis, the myoblasts were co-injected with fluorescent microspheres. 7 d later we sacrificed the mice and analyzed the behavior of the transplanted cells in the tissue by scoring the number of tdTomato-expressing myofibers that were generated by fusion events with the donor cells. Importantly, Wnt7a treatment increased the number of tdTomato-expressing myofibers by 119% (Fig. 5 B). To exclude that this effect is due to changes in the cell cycle status of the transplanted cells, we analyzed the

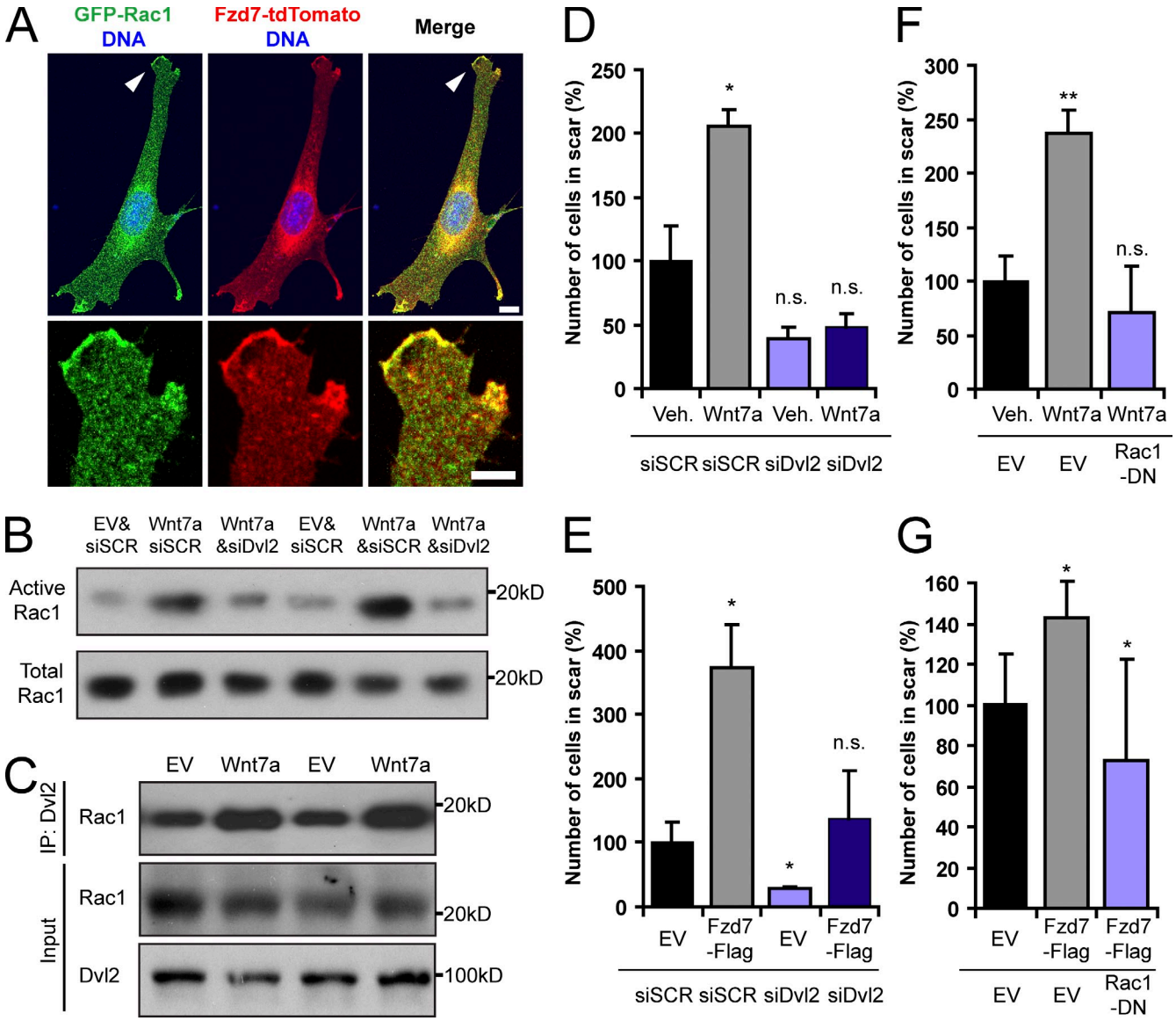

Figure 3. **Dvl2 and Rac1 are required for Wnt7a-induced cell migration.** (A) Fzd7-tdTomato colocalizes with GFP-Rac1 (arrowhead) in the periphery of C2C12 cells but not in cytoplasmic vesicles. Bar, 5 µm. (B) Rac1 activation assay of mouse primary myoblasts transduced with Wnt7a-HA (Wnt7a) retrovirus or an empty control virus (EV). In addition, all cells were either treated with an siRNA SMARTpool targeting Dvl2 (siDvl2) or with a scrambled control (siSCR). Total Rac1 is shown as a loading control. (C) Coimmunoprecipitation of Rac1 with Dvl2 in primary myoblasts that were infected with Wnt7a or EV. More Rac1 associates with Dvl2 in Wnt7a-expressing cells. (D) Scratch assay with mouse primary myoblasts that were Wnt7a or vehicle treated. The cells were also transfected with either siSCR or siDvl2. Error bars represent means ± SEM; $n = 3$. *, $P < 0.05$. n.s., no significant difference. (E) Scratch assay with mouse primary myoblasts that overexpress EV or Fzd7-Flag and that were treated with siDvl2 or siSCR. Error bars represent means ± SEM; $n = 3$. *, $P < 0.05$. (F) Dominant-negative Rac1 (Rac1-DN) prevents Wnt7a-induced mouse primary myoblast migration in scratch assays. Error bars represent means ± SEM; $n = 3$. **, $P < 0.01$. (G) Rac1-DN prevents Fzd7-Flag–induced mouse primary myoblast migration in scratch assays. Error bars represent means ± SEM; $n = 3$. *, $P < 0.05$.

proliferation of primary myoblasts after a 3-h exposure to various concentrations of Wnt7a. We did not observe any change in the rate of proliferation at any of the tested concentrations of Wnt7a over 5 d (Fig. S4 A). By contrast, the induction of canonical signaling with higher concentrations of Wnt3a reduced the proliferation of primary myoblasts (Fig. S4 B).

Taken together, these data support the conclusion that the increased number of tdTomato-expressing myofibers upon transplantation of Wnt7a-treated myoblasts is not due to increased proliferation and is a consequence of enhanced dispersal. The observed increase in numbers of highly (tdT+++) tdTomato-expressing myofibers proximal to the injection site after transplantation of untreated cells (Fig. 5, C–E) relative to Wnt7a-treated cells provides strong evidence in support of this conclusion. Importantly, the myofibers generated by fusion to Wnt7a-treated cells were weaker for tdTomato (tdT+), but higher in number and more spread out with respect to the injection site (Fig. 5, C and F). Thus, Wnt7a loading results in increased migration of the cells in the host muscle and lowers the chance for multiple fusion events to the same myofiber. Taken together, our experiments suggest that short exposure of myoblasts to Wnt7a dramatically enhances engraftment by promoting the tissue dispersion of the cells.

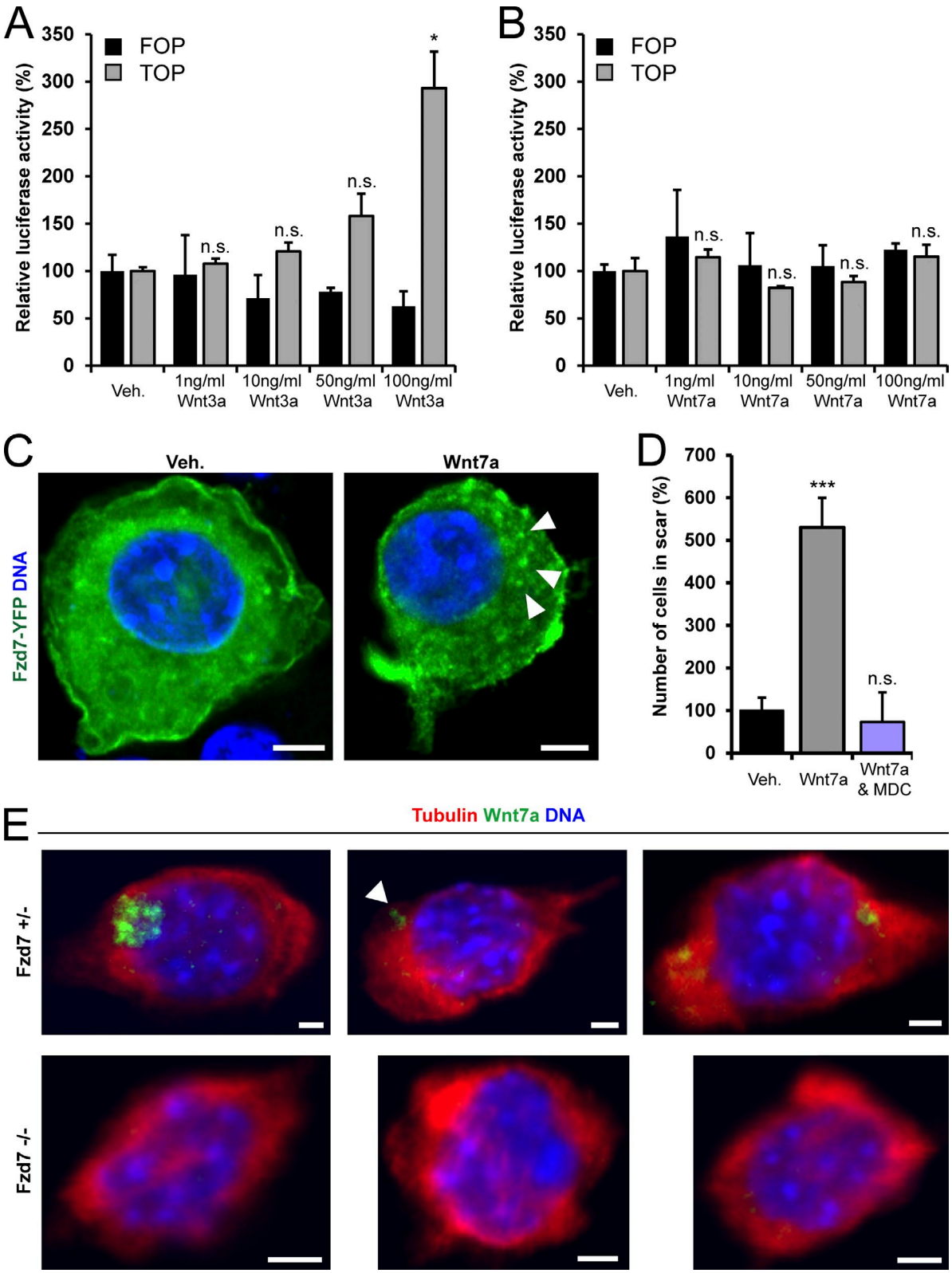

Figure 4. **The Fzd7/Wnt7a signal is strictly noncanonical.** (A) Wnt3a induces a dose-dependent increase in TOP-flash luciferase reporter activity in C2C12 cells. Error bars represent means ± SEM; $n = 3$. *, $P < 0.05$. n.s., no significant difference. (B) Wnt7a does not activate the TOP-flash reporter at any tested concentration. Error bars represent means ± SEM; $n = 3$. (C) Wnt7a treatment decreases the abundance of peripheral Fzd7-YFP and leads to its accumulation in intracellular clusters (arrowheads). Bar, 5 µm. (D) Inhibition of clathrin-dependent endocytosis with monodansylcadaverine (MDC) prevents Wnt7a-induced migration of primary myoblasts in scratch assays. Error bars represent means ± SEM; $n = 3$. ***, $P < 0.001$. (E) Substantial amounts of Wnt7a-HA are present in intracellular stores (arrowhead) 72 h after a 3-h exposure to conditioned supernatants produced in COS-1 cells (top). In primary myoblasts from Fzd7$^{-/-}$ mice, Wnt7a does not show such intracellular accumulation (bottom). Bars, 2 µm.

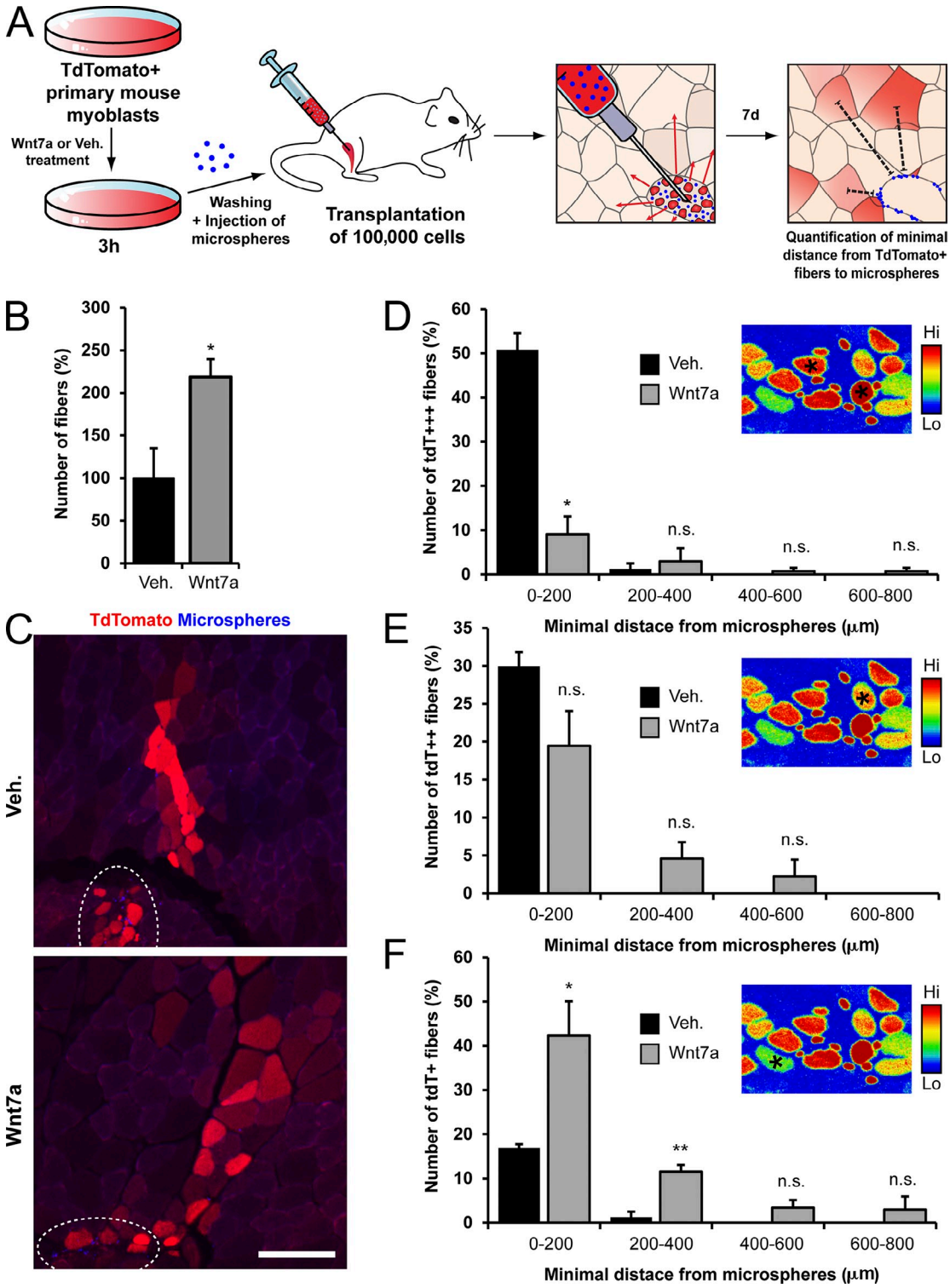

Figure 5. **Wnt7a loading increases myoblast dispersal in muscle tissue.** (A) Experimental scheme for the in vivo myoblast dispersal assay. Cells expressing tdTomato were treated with Wnt7a or vehicle for 3 h, washed, and transplanted into C57BL/6 mice. Blue fluorescent microspheres were co-injected to mark the injection site. After 7 d, the distance from the closest microsphere to myofibers expressing high (tdT+++), medium (tdT++), or low (tdT+) level of tdTomato was enumerated in muscle cross sections. (B) The total number of tdTomato-expressing myofibers generated by fusion with donor myoblasts was increased by Wnt7a treatment compared to vehicle. Error bars represent means ± SEM; $n = 3$. *, $P < 0.05$. (C) Representative images showing the abundance and fluorescent intensity of myofibers expressing tdTomato with respect to the injection site (outlined by a dashed oval). The injection site is marked by a high concentration of blue fluorescent microspheres. In the case of the cells that were treated with Wnt7a, the myofibers are more spread out and generally express reduced levels of tdTomato. Bar, 50 μm. (D–F) The minimal distance of tdT+++, tdT++, and tdT+ myofibers to the microspheres was measured in muscle cross-section according to the false-color image shown in the respective insets. Asterisks in the false-color images indicate the tdT fluorescence intensity of the fibers that were quantified. The data for the minimal distance from microspheres of the myofiber types was grouped into 200-μm bins. In the vehicle-treated condition, a large fraction of myofibers proximal to the injection site is tdT+++, whereas few distal tdT+ myofibers are present. The Wnt7a condition shows the opposite trend. Error bars represent means ± SEM; $n \geq 3$. *, $P < 0.05$; **, $P < 0.01$. n.s., no significant difference.

Wnt7a treatment enhances the outcome of cell therapy of dystrophic muscle

Because poor migration of myogenic cells upon intramuscular injection is a major hurdle for the development of cell-based therapies for muscular dystrophy (Skuk et al., 2007), we investigated whether ex vivo Wnt7a treatment of satellite cells before transplantation would enhance engraftment. We isolated 10,000 satellite cells from *Pax7-zsGreen* mice by fluorescent-activated cell sorting (Bosnakovski et al., 2008), treated them with Wnt7a for 3 h, washed them extensively, and transplanted them into the tibialis anterior muscle of immunosuppressed dystrophin-deficient *mdx* mice that were injured with cardiotoxin 2 d before the procedure (Fig. 6 A).

As determined by immunostaining for Pax7 and zsGreen in muscle sections, Wnt7a treatment enhanced engraftment of zsGreen-expressing cells into the recipient muscles by 69% after 3 wk (Fig. 6, B and C; and Fig. S4 C). Wnt7a treatment did not alter the proportion of zsGreen$^+$-engrafted cells that express Ki67 (Fig. S4 D), indicating that Wnt7a treatment does not alter the rate of in vivo proliferation. In addition, the number of endogenous satellite cells was not altered (Fig. S4 E), showing that resident satellite cells were not being stimulated by Wnt7a derived from the transplanted cells.

Under normal conditions, a portion of transplanted satellite cells will differentiate and fuse to muscle myofibers. In *mdx* mice, this process can be tracked by staining for restored dystrophin expression in muscle fibers. Using this assay, we observed that the number of myofibers expressing dystrophin increased on average by 486% after transplantation of Wnt7a-treated cells (Fig. 6, D and E). Demonstrating a stimulatory effect of Wnt7a on myogenic cell migration in vitro, clusters of dystrophin-expressing myofibers in muscles that were transplanted with Wnt7a-treated cells were on average located maximally 3.7 mm apart, while transplantation of untreated cells gave rise to clusters of dystrophin-expressing myofibers that were on maximally 2.2 mm apart on average (Fig. 6, F and G). We also observed that dystrophin-expressing myofibers arising after fusion with Wnt7a-treated cells were hypertrophic by 116% (Fig. 6, D and H). Importantly, transplantation of 3,000 satellite cells treated ex vivo with Wnt7a into *mdx* extensor digitorum longus muscles resulted in a striking 30% increase in twitch tension and in an 18% increase in maximal specific force generation when compared with the vehicle control (Fig. 6, I and J).

In a clinical setting, freshly isolated satellite cells are often not readily available. Therefore, we next tested the effect of 3 h Wnt7a loading on cultured primary mouse myoblasts that were subsequently transplanted into injured muscles of immunosuppressed *mdx* mice (Fig. S5 A). After transplantation of 100,000 cells, the number of dystrophin-expressing myofibers was increased by 72% in muscles that were injected with Wnt7a-treated myoblasts (Fig. S5 B). Moreover, dystrophin-expressing myofibers derived from Wnt7a-treated cells exhibited an 87% hypertrophy (Fig. S5 C). In addition, the mean maximal cluster distance increased from 1.5 mm for vehicle to 2.0 mm for Wnt7a (Fig. S5 D).

To ascertain that the improvement of engraftment efficiency is a unique property of Wnt7a, we also tested Wnt3a and Wnt5a loading of myoblasts before transplantation. Neither the number of dystrophin-expressing myofibers (Fig. S5 E) nor the mean maximal cluster distance (Fig. S5 F) was changed by these treatments. Taken together, these observations indicate that Wnt7a treatment can significantly enhance the outcome of cell therapy of skeletal muscle. Transplantation of dystrophic muscle with Wnt7a-loaded cells leads to an enhanced engraftment, enhanced tissue distribution of donor-derived myofibers, and improved force generation.

Ex vivo Wnt7a treatment stimulates human myoblast transplantation

To investigate the translational relevance of our findings, we assessed whether Wnt7a treatment is also effective in human primary myoblasts. Both Wnt7a treatment and Fzd7 overexpression significantly increased human myoblast migration, whereas Rac-DN prevented this effect (Fig. 7, A and B).

To test the in vivo effectiveness of Wnt7a on human myoblasts, we used the same experimental paradigm that we previously used for mouse myoblasts (Fig. 7 C). Transplantation of 100,000 human myoblasts, treated ex vivo with Wnt7a for 3 h, resulted in a 226% increase in the number of dystrophin-expressing myofibers in muscles of immunosuppressed *mdx* mice when compared with vehicle (Fig. 7 D). Myofibers arising from fusion of mouse myofibers to Wnt7a-treated human myoblasts exhibited a 29% increase in fiber feret (Fig. 7 E). Moreover, the mean maximal distance between dystrophin-expressing myofiber clusters increased from 1.8 mm under the vehicle condition to 3.0 mm for Wnt7a treatment (Fig. 7 F). Therefore, we conclude that the Wnt7a-mediated induction of motility of myogenic cells is conserved in humans.

Taken together, ex vivo Wnt7a treatment enhances the migration and tissue dispersion of both mouse and human myogenic cells through Dvl2 and the small GTPases. This effect is most pronounced in, but not limited to, satellite cells, indicating that committed myogenic progenitors readily activate noncanonical signaling in response to Wnt7a. We conclude that Wnt7a has several therapeutically attractive properties that modulate muscle regeneration at multiple levels, including the stimulation of motility and engraftment (Fig. 8).

Discussion

Strategies to treat progressive degenerative muscle diseases include the genetic correction of affected muscle fibers and the restoration of tissue regenerative capacity (Wang et al., 2013). The ability of myogenic cells to add their nuclei to the syncytial muscle fibers through fusion makes them an ideal candidate for cell therapy of genetic diseases that affect myofiber stability or function (Bentzinger et al., 2012; Wang and Rudnicki, 2012). Moreover, life-long muscle hypertrophy as a consequence of transplanting a small number of satellite cells raises hope for the use of these cells as a therapeutic option for conditions such as burns, cancer cachexia, and sarcopenia that are accompanied by uncontrolled catabolism of muscle protein (Hall et al., 2010).

In humans, satellite cells account for less than 5% of total myofiber nuclei (Lindström and Thornell, 2009). In addition, the amount of tissue that can be obtained from a muscle biopsy

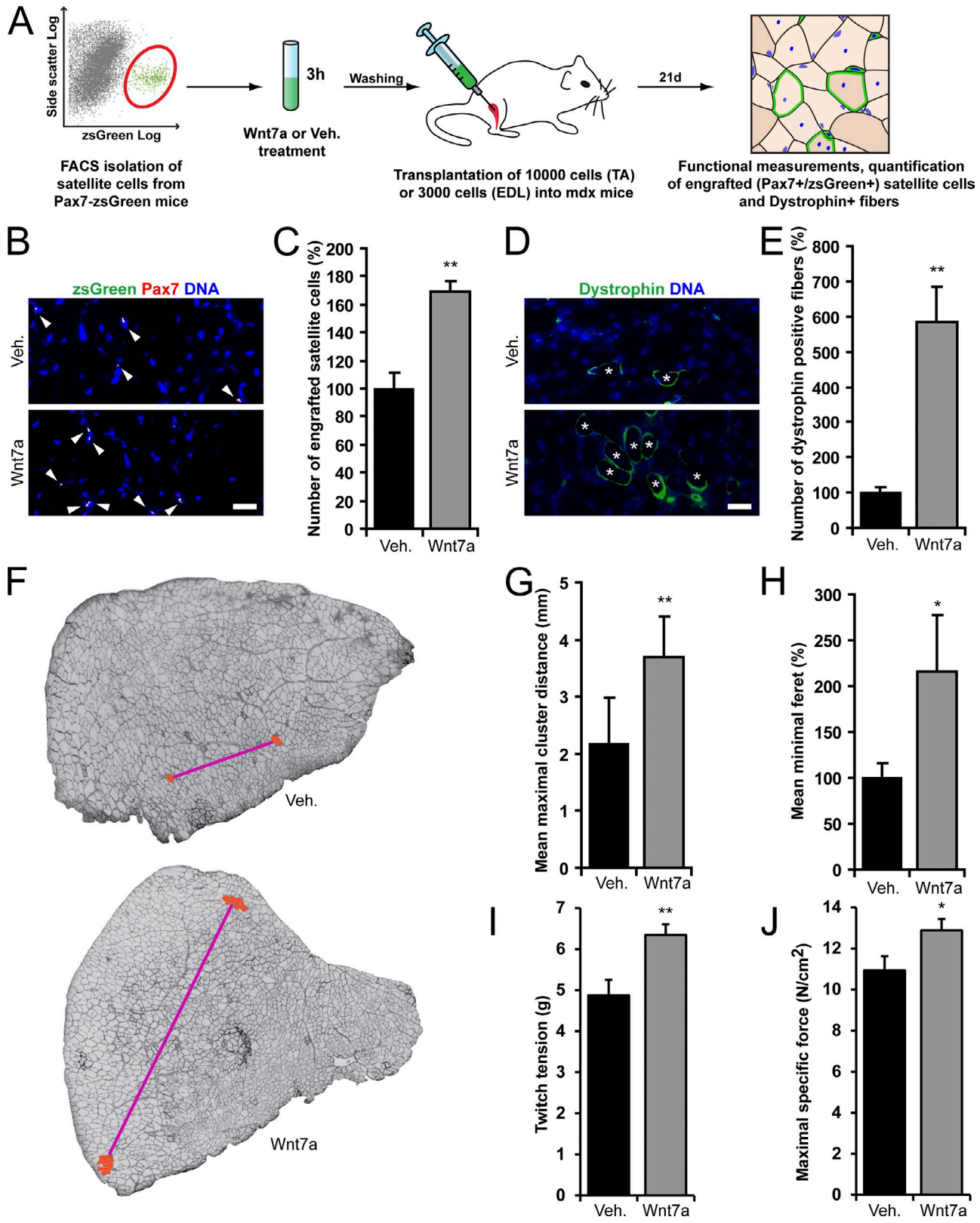

Figure 6. **Wnt7a-loaded satellite cells have an enhanced engraftment potential.** (A) Schematic of the isolation, ex vivo treatment, and transplantation of satellite cells from Pax7-zsGreen mice. (B) Representative pictures showing engraftment of zsGreen- and Pax7-expressing donor-derived cells that were either Wnt7a or vehicle treated. Bar, 20 µm. (C) Quantification of engraftment of Wnt7a- or vehicle-treated donor satellite cells (Pax7$^+$/zsGreen$^+$, arrowheads in B). Error bars represent means ± SEM; $n = 3$. **, $P < 0.01$. (D) Representative images showing dystrophin-expressing myofibers (asterisks) derived from transplanted Wnt7a or vehicle-treated satellite cells. Bar, 20 µm. (E) Quantification of myofibers expressing dystrophin after transplantation of Wnt7a- or vehicle-treated satellite cells. Error bars represent means ± SEM; $n = 3$. **, $P < 0.01$. (F) Engrafted satellite cells form clusters of dystrophin-expressing myofibers in host *mdx* muscles. The photographs show the tibialis anterior muscle that was injected with Wnt7a- or vehicle-treated cells. The

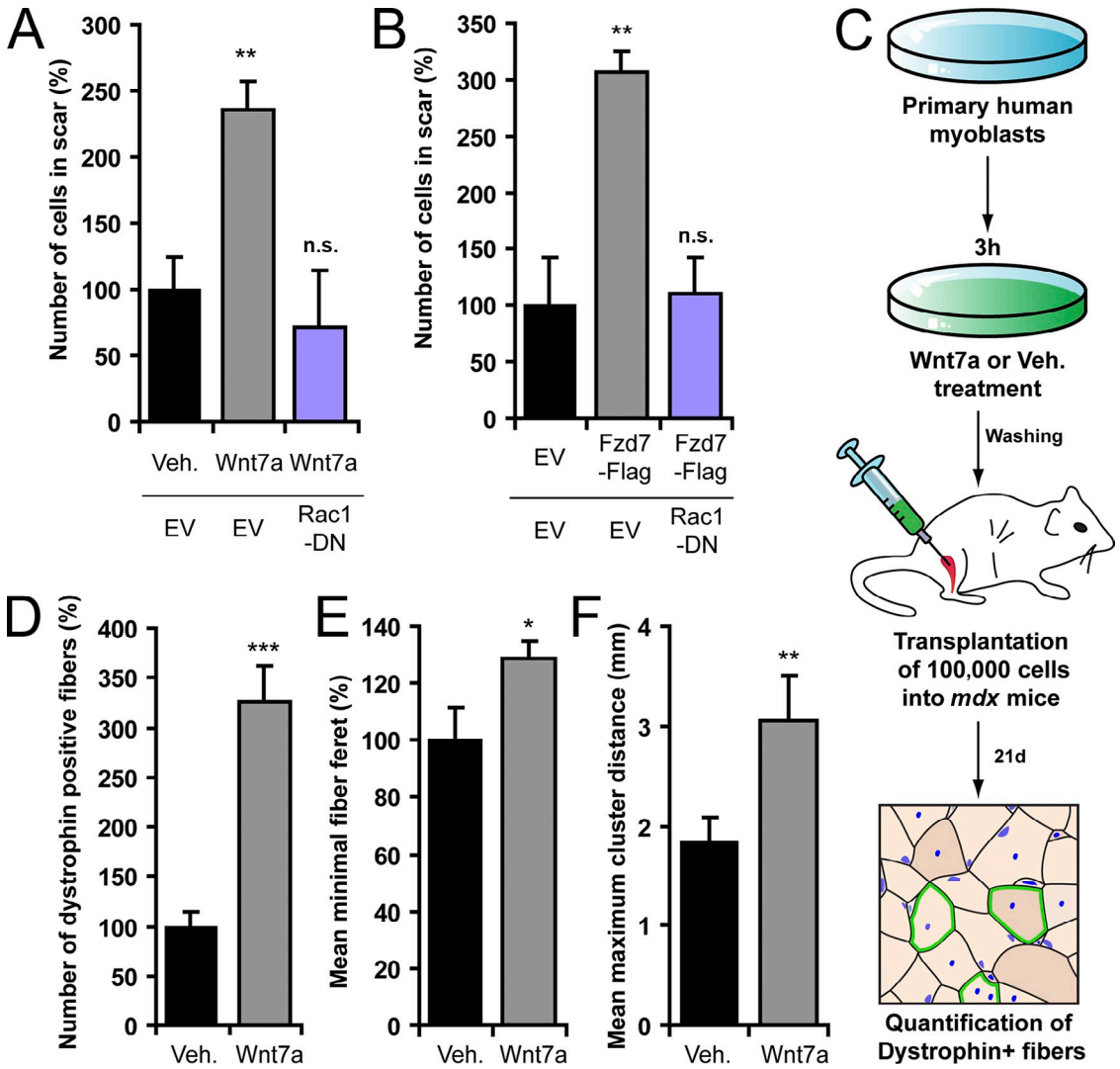

Figure 7. **Wnt7a stimulates dispersal of human primary myoblasts.** (A) Scratch assay with human myoblasts. Wnt7a treatment significantly increases cell migration into the scar and expression of Rac1-DN prevents this effect. Error bars represent means ± SEM; $n = 3$. **, $P < 0.01$. (B) Fzd7-Flag increases human myoblast migration and Rac1-DN prevents this effect. Error bars represent means ± SEM; $n = 3$. **, $P < 0.01$. n.s., no significant difference. (C) Strategy used for Wnt7a or vehicle treatment and subsequent transplantation of human primary myoblasts into *mdx* mice. (D) Number of dystrophin-expressing myofibers after transplantation of Wnt7a- or vehicle-treated cells. Error bars represent means ± SEM; $n \geq 4$. ***, $P < 0.001$. (E) Minimal myofiber Feret of dystrophin-expressing myofibers generated from fusion with Wnt7a- or vehicle-treated human primary myoblasts. Error bars represent means ± SEM; $n = 3$. *, $P < 0.05$. (F) Mean maximum cluster difference in muscles transplanted with Wnt7a- or vehicle-treated human primary myoblasts. Error bars represent means ± SEM; $n \geq 4$. **, $P < 0.01$.

is relatively small. Therefore, the availability of sufficient donor cells is a major obstacle for the effective therapy of affected muscle groups. Compounding this problem, in vitro expansion of satellite cells profoundly impairs their stem cell character and decreases the efficiency of engraftment several fold (Ikemoto et al., 2007). In agreement with these observations, we show that the effects of Wnt7a on transplanted satellite cells are much more profound when compared with human and mouse myoblasts (compare Fig. 6 with Fig. 7 and Fig. S5). Nevertheless, Wnt7a was also highly beneficial for the outcome of myoblast transplantation. After ex vivo Wnt7a treatment, human myoblasts generated >200% dystrophin-expressing myofibers that were also distributed more evenly throughout the tissue (Fig. 7, D and F). This suggests that the dose of cells required for therapy will be threefold more effective if they are treated with Wnt7a before transplantation.

The transplantation of ex vivo Wnt7a-loaded cells into dystrophic muscles results in a significant increase in both the twitch tension and the maximal specific force, when compared

distance between the two maximally spaced clusters of dystrophin-expressing myofibers (highlighted in red) is indicated with a magenta line. (G) Quantification of the maximal cluster distance in muscles injected with Wnt7a- or vehicle-treated cells. Error bars represent means ± SEM; $n \geq 4$. **, $P < 0.01$. (H) Minimal feret measurements of dystrophin-expressing myofibers in host muscles. Myofibers that had fused with a Wnt7a-treated cell become hypertrophic. Error bars represent means ± SEM; $n = 3$. *, $P < 0.05$. (I) Quantification of the twitch force tension of *mdx* muscles injected with Wnt7a- or vehicle-treated cells. Error bars represent means ± SEM; $n \geq 7$. **, $P < 0.01$. (J) Maximal specific force generated by *mdx* muscles injected with Wnt7a- or vehicle-treated cells. Error bars represent means ± SEM; $n \geq 7$. *, $P < 0.05$.

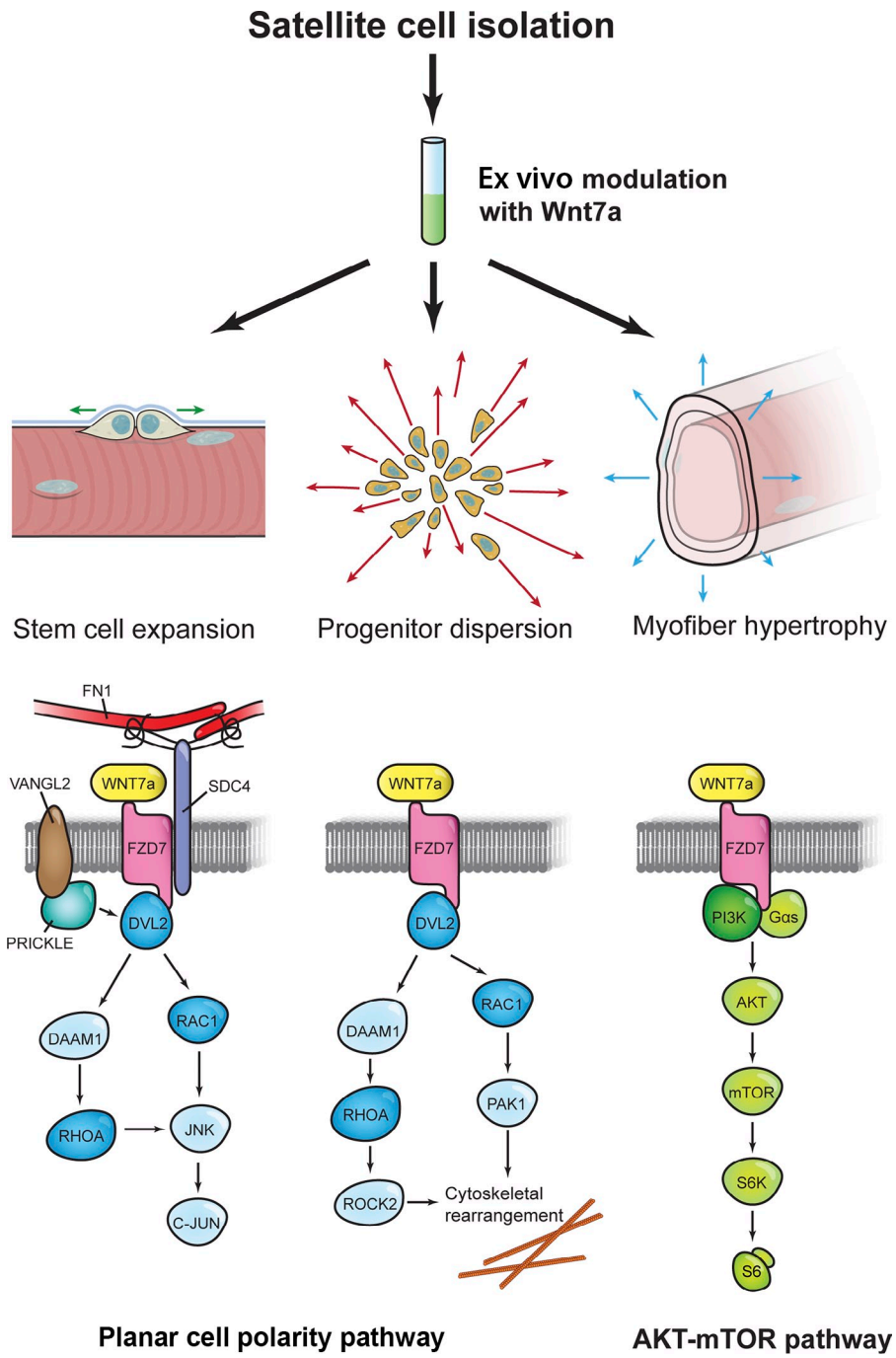

Figure 8. **Molecular mechanisms of ex vivo Wnt7a modulation.** Upon stimulation, Wnt7a induces the symmetric proliferation of Myf5-independent satellite cells in conjunction with fibronectin (FN1), syndecan-4 (SDC4) and Vangl2 through the planar cell polarity pathway. In myogenic progenitors, Wnt7a also facilitates Rac1-mediated cell polarization and migration. Fusion of Wnt7a-treated cells activates the AKT–mTOR pathway, leading to myofiber hypertrophy. Therefore, Wnt7a acts on three levels to facilitate the outcomes of cell therapy: (1) it boosts stem cell number, (2) facilitates their dispersion in the host tissue, and (3) leads to muscle growth.

with vehicle (Fig. 6, I and J). The enhanced twitch tension, a direct measure of muscle strength, is conceivably the result of myofiber hypertrophy induced by fusion of Wnt7a-loaded cells (Fig. 6, H and I). By contrast, the improved contraction quality under tetanic stimulation likely reflects the higher number of more evenly distributed dystrophin-expressing myofibers in the Wnt7a condition (Fig. 6, E and J).

Directional cell migration is a phenomenon that has previously been described to be controlled by noncanonical Wnt signaling (Seifert and Mlodzik, 2007). In agreement with these observations, our experiments demonstrate that the enhanced tissue dispersion of Wnt7a-stimulated cells is due to directed migration (Fig. 2, H and I) and does not involve induction of proliferation (Fig. S4 A). Importantly, the effect of Wnt7a on the migration of myogenic progenitors is strictly β-catenin independent (Fig. S2 B and Fig. 4 B) and involves effectors of noncanonical Wnt signaling such as Dvl2 and small GTPases (Fig. 3 and Fig. S3 D).

It has been shown that a necrotic core can form at the injection site after transplantation of myogenic cells (Skuk et al., 2007). This will ultimately lead to increased cell death of transplanted cells. An enhanced ability of cells to migrate away from the injection site to prevent or escape necrotic cell death should therefore contribute to the increased engraftment in muscles that were transplanted with Wnt7a-treated cells.

We observed that both Fzd7 and its downstream effector Rac1 showed a characteristic subcellular localization within

vesicles in the cytoplasm and accumulated in the periphery of the cell (Fig. 1, B and C; and Fig. 3 A). Intriguingly, Fzd7 colocalized with Rac1 in the cellular periphery, whereas intracellular vesicle–associated Fzd7 did not colocalize with Rac1 (Fig. 3 A). Using live imaging of single cells, we observed that Fzd7-YFP is dynamically rearranged at the leading edge of migrating cells (Fig. 1 C and Video 1). This suggests that Fzd7 locally activates Rac1 to facilitate directed migration. Furthermore, the localization of Fzd7 at the leading edge of migrating cells may allow the cells to respond to gradients of Wnt. In agreement with this hypothesis, Vangl2, a core component of planar cell polarity signaling in satellite stem cells, has been shown to form a Wnt-induced receptor complex with Ror2 to sense Wnt gradients. However, a direct involvement of Vangl2 in myogenic progenitor migration remains to be defined (Gao et al., 2011).

Endocytosis of Fzd receptors upon Wnt stimulation has been shown to be required for noncanonical Wnt signaling (Yu et al., 2007; Sato et al., 2010). In the case of Fzd2, clathrin-mediated endocytosis is a prerequisite for the activation of Rac1 (Sato et al., 2010). Our results suggest that clathrin-dependent endocytosis is also required for the induction of Wnt7a/Fzd7 signaling (Fig. 4 D). In agreement with this idea, we observed that a large fraction of Fzd7 localizes to intracellular vesicles that seem attached to the tubulin cytoskeleton (Fig. 1 B). Wnt7a treatment leads to partitioning of Fzd7 away from the cellular periphery into these intracellular structures (Fig. 4 C). We also observed that myogenic cells readily endocytose Wnt7a in a Fzd7-dependent manner after only a few hours of exposure (Fig. 4 E and Fig. S3 E). Interestingly, in tumor cells it has been shown that an antibody directed to Fzd7 is quickly endocytosed and accumulates in multivesicular bodies (Pode-Shakked et al., 2011) reminiscent of the ones we observed for Wnt7a in myoblasts (Fig. 4 E and Fig. S3 E). Unexpectedly, intracellular Wnt7a could be detected in the cells for periods longer than 72 h after internalization. Muscle fibers fused to such Wnt7a-loaded cells become hypertrophic (Fig. 6 H, Fig. S5 C, and Fig. 7 E). Therefore, we hypothesize that Wnt7a can be released from intracellular storage to induce the signaling events leading to the hypertrophic response.

Due to their lipid modifications and other unique biochemical properties, Wnt proteins are notoriously difficult to purify (Willert and Nusse, 2012). This undoubtedly complicates their use as a therapeutic. However, we observed that exposure of cells to Wnt7a in the nanomolar range was sufficient to produce extremely long-lasting effects. It is therefore likely that sufficient production of pharmaceutical grade Wnt7a for standardized therapies can be achieved. Of note, our laboratory recently demonstrated that a truncated Wnt7a, consisting of the C-terminal 137 aa and lacking palmitoylation sites, retains full biological activity in skeletal muscle (von Maltzahn et al., 2013b). Thus, large-scale manufacture of Wnt7a variants for use as a biological appears feasible.

In this study we demonstrate that ex vivo Wnt7a loading is a highly efficient means to modulate mouse and human myogenic cells before transplantation. Our work demonstrates that binding of Wnt7a to Fzd7 leads to an activation of noncanonical Wnt signaling, resulting in directed cell migration and enhanced engraftment. Moreover, Wnt7a-loaded cells are remarkably effective in increasing the growth and strength of dystrophic muscle. Taken together, our work identifies for the first time a viable pharmacological means to significantly improve the outcome of stem cell therapy for muscle diseases.

Materials and methods

Mice and animal care

Pax7-CreER;R26R-tdTomato mice were generated as described previously (Yin et al., 2013a). In brief, mice expressing a tamoxifen-inducible Cre from the endogenous Pax7 promoter were bred with mice carrying a loxP-flanked STOP cassette followed by tdTomato in the ROSA26 locus. Pax7-zsGreen mice were generated by replacing the Pax7 coding sequence with the sequence encoding ZsGreen (Bosnakovski et al., 2008). Fzd7 knockout mice were generated by replacing the Fzd7 coding region with a nuclear-localized lacZ (Yu et al., 2012). *mdx* mice were obtained from The Jackson Laboratory. All experiments were performed in accordance with University of Ottawa guidelines for animal handling and care.

Transplantation

Transplantation of zsGreen-expressing satellite cells or myoblasts into *mdx* mice was performed as described previously (Bentzinger et al., 2013b). In brief, cells were resuspended in 0.9% NaCl and transplanted into the muscles of FK506-immunosupressed mice that had been injured 2 d before. Before transplantation the cells were treated for 3 h with Wnt7a, Wnt5a, or Wnt3a (R&D Systems) at a concentration of 50 ng/ml for freshly isolated satellite cells or with 100 ng/ml for cultured cells. Myoblasts expressing tdTomato were transplanted into uninjured muscles of C57BL/6 mice that were implanted with an osmotic pump (Alzet) delivering FK506 (Sigma-Aldrich) at 2.5mg/kg/day 3 d before the transplantations. In some experiments the injection site was marked with blue fluorescent microspheres (2 µm; Life Technologies) that were added at a concentration of 1:100 (vol/vol) to the cell suspension. 10 µl of the cell-microsphere suspension was injected into the tibialis anterior of each mouse using a syringe (Hamilton Company).

Muscle force measurements

Extensor digitorum longus muscles were isolated three weeks after transplantation and attached to an electrode and a force sensor (Aurora Scientific), and incubated at 25°C in buffered physiological saline (Krebs-Ringer) supplemented with glucose and oxygen. Twitch force was determined after a single electrical stimulus, whereas maximal force was generated by electrical stimulation at 100 Hz for 500 ms. Thereafter, muscle length and weight were measured and specific muscle force was calculated ([maximal force × optimal fiber length × muscle density]/muscle mass).

Live imaging

Single-cell imaging of cells transfected with Fzd7-YFP or YFP was performed on a microscope (Axio Observer.Z1; Carl Zeiss) equipped with a confocal laser scanner (LSM510 META; Carl Zeiss) and a Plan Apochromat 63×/1.40 NA oil DIC M27 objective (Carl Zeiss) under 5% CO_2 at 37°C in phenol-red free DMEM (Life Technologies) containing 10% FBS. Image acquisition was performed using Zen software (Carl Zeiss). Imaging of satellite cells on fibers was performed as described previously (Siegel et al., 2009). In brief, time-lapse microscopy of satellite cells on single collagen-embedded muscle fibers was performed using an inverted microscope (DMI 5100; Leica) and MetaMorph 7.6.1 software (Molecular Devices) with time points being acquired every 7 min in a stage-top incubator (LiveCell Imaging). ImageJ (National Institutes of Health) analyzed the time-lapse data to calculate the velocity, defined as distance (µm)/time (h), between time points, and the average velocity of each cell was calculated. The maximum velocity is defined as the highest velocity obtained by a single cell during the tracking period. For live imaging of satellite cells on single fibers, Wnt7a was used at a concentration of 1.5 µg/ml.

Isolation of satellite cells and culture of primary myoblast

For myoblast culture and transplantation, satellite cells were FACS purified from Pax7-zsGreen mice through gating for zsGreen and Hoechst using a cell sorter (MoFlo XDP, Beckman Coulter; Bentzinger et al., 2013b). To derive primary myoblasts, the cells were then plated on collagen-coated dishes (BD) in Ham's F10 medium supplemented with 20% FBS and 5 ng/ml of basic FGF (EMD Millipore). C2C12 cells and human myoblasts were cultured in DMEM supplemented with 10% FBS (von Maltzahn et al.,

2012). For in vitro morphology quantifications, Wnt7a was used at a concentration of 50 ng/ml.

Scratch assays

After plasmid transfection or application of Wnts (R&D Systems), the cells were treated with 50 µg/ml mitomycin-C for 2 h. Subsequently, the monolayer of cells was scraped in a straight line. The plates were then extensively washed with culture medium and incubated for 24 h before analysis. Analysis was performed using DAPI staining after matching the reference points, and enumeration of DAPI-stained nuclei in the scar was performed. Unless indicated otherwise, Wnt7a and Wnt3a were used at a concentration of 100 ng/ml in scratch assays. Monodansylcadaverine (30432; Sigma-Aldrich) was used in scratch assays at a concentration of 50 µm.

Western blotting and immunoprecipitation

For coimmunoprecipitation (CoIP) experiments and the Rac1 activation assay, satellite cell–derived primary myoblasts were infected with retroviruses generated from empty pHAN or from pHAN-Wnt7a-HA (Kuroda et al., 2013). Dvl2 knockdown was performed with an ON-TARGETplus siRNA SMARTpool (L-040921-01, Thermo Fisher Scientific; Wu et al., 2008) using Lipofectamine RNAiMAX (Life Technologies) according to the manufacturer's instructions. As a control for the knockdown, a nonsilencing siRNA SMARTpool was used (D-001810-10; Thermo Fisher Scientific). Cell extracts were obtained through RIPA buffer lysis in the presence of a protease inhibitor cocktail (Nacalai Tesque). For CoIP of Rac1 with Dvl2, rabbit anti-Dvl2 antibody was coupled to protein A–Dynabeads (Life Technologies). Denaturing SDS-PAGE was performed using standard techniques. Rac1 activation assay was performed according to the manufacturer's instructions (Termo Fisher Scientific).

Immunostaining and antibodies

Muscles frozen in liquid nitrogen were cut into 12-µm cross sections. Cross sections and cells were either fixed with 100% ethanol or 2% PFA for 5 min, permeabilized with 0.1% Triton X-100/0.1 M glycine/PBS for 10 min, blocked with 5% horse serum in PBS for several hours, and incubated with specific primary antibody in blocking buffer overnight at 4°C. Samples were subsequently washed with PBS and stained with appropriate fluorescently labeled secondary antibodies for 1 h at room temperature. After washing with PBS, samples were mounted with Permafluor (Thermo Fisher Scientific). Antibodies were as follows: chicken anti-GFP (ab13970; Abcam), mouse anti-Pax7 (Developmental Studies Hybridoma Bank [DSHB]), mouse anti-dystrophin (7A10; DSHB), mouse anti-Rac1 (05-389; EMD Millipore), mouse anti-tubulin (T9026; Sigma-Aldrich), rabbit anti-Dvl2 (3224; Cell Signaling Technology), rabbit anti-zsGreen (632474; Takara Bio Inc.), and rabbit anti-laminin (L9393; Sigma-Aldrich), rabbit anti-HA (07-221; EMD Millipore). Fluorochromes coupled to secondary antibodies were Alexa Fluor 488, 546, and 647. Images of immunostainings were taken at room temperature on a microscope (Axio Observer.Z1; Carl Zeiss) equipped with a confocal laser scanner (LSM510 META; Carl Zeiss) and an EC Plan-Neofluar 20×/0.50 NA M27, EC Plan-Neofluar 40×/1.30 NA oil DIC M27, and Plan Apochromat 63×/1.40 NA oil DIC M27 objective (all from Carl Zeiss).

Real-time PCR

Total RNA was isolated (NucleoSpin RNA II; Macherey-Nagel). Reverse transcription was performed using a mixture of oligodT and random hexamer primers (iScript cDNA Synthesis kit; Bio-Rad Laboratories). SYBR Green real-time PCR analysis (iQ SYBR Supermix; Bio-Rad Laboratories) was performed using a real-time thermocycler (Mx300P; Agilent Technologies). The following primers were used: Dvl2 sense: 5′-ACGACGATGCTGTACGAGTG-3′; Dvl2 anti-sense: 5′-CGAGGGAGGGTGAAGTAGG-3′; Fzd7 sense: 5′-GCTTCCTAGGTGAGCGTGAC-3′; and Fzd7 anti-sense: 5′-AACCCGACAGGAAGATGATG-3′.

Plasmids and transfection

The UBC-Fzd7-Flag (Fzd7-Flag; backbone: pLenti-III-UBC), CMV-Fzd7-EYFP (Fzd7-YFP; backbone: pEYFP-N1), CMV-Fzd3-EYFP (Fzd3-YFP; backbone: pEYFP-N1), CMV-EYFP (YFP; backbone: pEYFP-N1), CMV-EGFP-Rac1-wt (GFP-Rac1, 12980; Addgene; backbone: pcDNA3-EGFP), CMV-EGFP-Rac1-T17N (Rac1-DN, 12982; Addgene; backbone: pcDNA3-EGFP), CMV-EGFP-RhoA-T19N (RhoA-DN, 12967; Addgene; backbone: pcDNA3-EGFP), and CMV-EGFP-Cdc42-T17N (Cdc42-DN, 12976; Addgene; backbone: pcDNA3-EGFP) constructs have been described previously (Subauste et al., 2000; von Maltzahn et al., 2011; Bentzinger et al., 2013a). The Fzd7-tdtomato plasmid was generated by replacing the C-terminal YFP in Fzd7-YFP with tdTomato. For TOP-flash and FOP-flash the TCF reporter plasmid kit (17-285; EMD Millipore) was used with the dual-luciferase reporter assay system (E1960; Promega). For normalization, pGL4.74[hRluc/TK] (E6921; Promega) was cotransfected. For TOP-flash and FOP-flash assays the cells were transfected with the GenJet Lipofection reagent (SL100499; SignaGen). Otherwise, Lipofectamine 2000 (11668019; Life Technologies) was used for all transfections.

Statistical analysis

Densitometry of gray values from Western blots was performed with ImageJ software. Compiled data are expressed as the mean ± SEM. Experiments were done with a minimum of three biological replicates. For statistical comparison of two conditions, the Student's *t* test was used. The level of significance is indicated as follows: ***, $P < 0.001$; **, $P < 0.01$; *, $P < 0.05$.

Online supplemental material

Fig. S1 shows that Wnt7a polarizes myogenic cell types. Fig. S2 shows Fzd7 mRNA levels in Fzd7 knockout muscle tissue and dose dependency of Wnt7a-mediated cell migration. Fig. S3 shows gray value quantification of Western blots, Dvl2 mRNA levels after siRNA knockdown, and Wnt7a endocytosis in C2C12 cells. Fig. S4 shows that Wnt7a does not influence the cell cycle, increases engraftment of satellite cells, and does not alter the number of endogenous satellite cells. Fig. S5 shows that Wnt7a loading improves the engraftment of mouse primary myoblasts. Videos 1 and 2 show, respectively, Fzd7-YFP accumulation in the periphery of migrating cells, but a lack of polarized localization for YFP alone. Video 3 shows a Wnt7a-dependent increase in the mean velocity of satellite cells. Online supplemental material is available at http://www.jcb.org/cgi/content/full/jcb.201310035/DC1.

We thank J. Nathans for providing us with the Fzd7 knockout mice and D. Wilson for technical assistance.

C.F. Bentzinger is supported by a grant from the Swiss National Science Foundation. Y.X. Wang is supported by fellowships from QEII-GSST and the Canadian Institutes of Health Research. N.A. Dumont is supported by Canadian Institutes of Health Research. This work was supported by grants to M.A. Rudnicki from the Canadian Institutes for Health Research, the Muscular Dystrophy Association, the National Institutes of Health, the Canadian Stem Cell Network, the Ontario Ministry of Research and Innovation, and the Canada Research Chair Program; and to D.D.W. Cornelison from the National Institutes of Health. M.A. Rudnicki is a founding scientist with Fate Therapeutics, who are developing Wnt7a as a therapeutic agent.

The remaining authors declare no competing financial interests.

Submitted: 7 October 2013
Accepted: 5 March 2014

References

Bareja, A., and A.N. Billin. 2013. Satellite cell therapy - from mice to men. *Skelet Muscle*. 3:2. http://dx.doi.org/10.1186/2044-5040-3-2

Bentzinger, C.F., Y.X. Wang, J. von Maltzahn, and M.A. Rudnicki. 2012. The emerging biology of muscle stem cells: implications for cell-based therapies. *Bioessays*. 35:231–241. http://dx.doi.org/10.1002/bies.201200063

Bentzinger, C.F., S. Lin, K. Romanino, P. Castets, M. Guridi, S. Summermatter, C. Handschin, L.A. Tintignac, M.N. Hall, and M.A. Rüegg. 2013a. Differential response of skeletal muscles to mTORC1 signaling during atrophy and hypertrophy. *Skelet Muscle*. 3:6. http://dx.doi.org/10.1186/2044-5040-3-6

Bentzinger, C.F., Y.X. Wang, J. von Maltzahn, V.D. Soleimani, H. Yin, and M.A. Rudnicki. 2013b. Fibronectin regulates Wnt7a signaling and satellite cell expansion. *Cell Stem Cell*. 12:75–87. http://dx.doi.org/10.1016/j.stem.2012.09.015

Bosnakovski, D., Z. Xu, W. Li, S. Thet, O. Cleaver, R.C. Perlingeiro, and M. Kyba. 2008. Prospective isolation of skeletal muscle stem cells with a Pax7 reporter. *Stem Cells*. 26:3194–3204. http://dx.doi.org/10.1634/stemcells.2007-1017

de Forges, H., A. Bouissou, and F. Perez. 2012. Interplay between microtubule dynamics and intracellular organization. *Int. J. Biochem. Cell Biol.* 44:266–274. http://dx.doi.org/10.1016/j.biocel.2011.11.009

Gao, B., H. Song, K. Bishop, G. Elliot, L. Garrett, M.A. English, P. Andre, J. Robinson, R. Sood, Y. Minami, et al. 2011. Wnt signaling gradients establish planar cell polarity by inducing Vangl2 phosphorylation through Ror2. *Dev. Cell*. 20:163–176. http://dx.doi.org/10.1016/j.devcel.2011.01.001

Hall, J.K., G.B. Banks, J.S. Chamberlain, and B.B. Olwin. 2010. Prevention of muscle aging by myofiber-associated satellite cell transplantation. *Sci. Transl. Med.* 2:57ra83. http://dx.doi.org/10.1126/scitranslmed.3001081

Hoggatt, J., P. Singh, J. Sampath, and L.M. Pelus. 2009. Prostaglandin E2 enhances hematopoietic stem cell homing, survival, and proliferation. *Blood*. 113:5444–5455. http://dx.doi.org/10.1182/blood-2009-01-201335

Ikemoto, M., S. Fukada, A. Uezumi, S. Masuda, H. Miyoshi, H. Yamamoto, M.R. Wada, N. Masubuchi, Y. Miyagoe-Suzuki, and S. Takeda. 2007. Autologous transplantation of SM/C-2.6(+) satellite cells transduced with micro-dystrophin CS1 cDNA by lentiviral vector into *mdx* mice. *Mol. Ther.* 15:2178–2185. http://dx.doi.org/10.1038/sj.mt.6300295

Jenq, R.R., and M.R. van den Brink. 2010. Allogeneic haematopoietic stem cell transplantation: individualized stem cell and immune therapy of cancer. *Nat. Rev. Cancer*. 10:213–221. http://dx.doi.org/10.1038/nrc2804

Kuang, S., K. Kuroda, F. Le Grand, and M.A. Rudnicki. 2007. Asymmetric self-renewal and commitment of satellite stem cells in muscle. *Cell*. 129:999–1010. http://dx.doi.org/10.1016/j.cell.2007.03.044

Kuang, S., M.A. Gillespie, and M.A. Rudnicki. 2008. Niche regulation of muscle satellite cell self-renewal and differentiation. *Cell Stem Cell*. 2:22–31. http://dx.doi.org/10.1016/j.stem.2007.12.012

Kuroda, K., S. Kuang, M.M. Taketo, and M.A. Rudnicki. 2013. Canonical Wnt signaling induces BMP-4 to specify slow myofibrogenesis of fetal myoblasts. *Skelet Muscle*. 3:5. http://dx.doi.org/10.1186/2044-5040-3-5

Le Grand, F., A.E. Jones, V. Seale, A. Scimè, and M.A. Rudnicki. 2009. Wnt7a activates the planar cell polarity pathway to drive the symmetric expansion of satellite stem cells. *Cell Stem Cell*. 4:535–547. http://dx.doi.org/10.1016/j.stem.2009.03.013

Lindström, M., and L.E. Thornell. 2009. New multiple labelling method for improved satellite cell identification in human muscle: application to a cohort of power-lifters and sedentary men. *Histochem. Cell Biol.* 132:141–157. http://dx.doi.org/10.1007/s00418-009-0606-0

Molenaar, M., M. van de Wetering, M. Oosterwegel, J. Peterson-Maduro, S. Godsave, V. Korinek, J. Roose, O. Destrée, and H. Clevers. 1996. XTcf-3 transcription factor mediates beta-catenin-induced axis formation in *Xenopus* embryos. *Cell*. 86:391–399. http://dx.doi.org/10.1016/S0092-8674(00)80112-9

North, T.E., W. Goessling, C.R. Walkley, C. Lengerke, K.R. Kopani, A.M. Lord, G.J. Weber, T.V. Bowman, I.H. Jang, T. Grosser, et al. 2007. Prostaglandin E2 regulates vertebrate haematopoietic stem cell homeostasis. *Nature*. 447:1007–1011. http://dx.doi.org/10.1038/nature05883

Pode-Shakked, N., O. Harari-Steinberg, Y. Haberman-Ziv, E. Rom-Gross, S. Bahar, D. Omer, S. Metsuyanim, E. Buzhor, J. Jacob-Hirsch, R.S. Goldstein, et al. 2011. Resistance or sensitivity of Wilms' tumor to anti-FZD7 antibody highlights the Wnt pathway as a possible therapeutic target. *Oncogene*. 30:1664–1680. http://dx.doi.org/10.1038/onc.2010.549

Relaix, F., D. Montarras, S. Zaffran, B. Gayraud-Morel, D. Rocancourt, S. Tajbakhsh, A. Mansouri, A. Cumano, and M. Buckingham. 2006. Pax3 and Pax7 have distinct and overlapping functions in adult muscle progenitor cells. *J. Cell Biol.* 172:91–102. http://dx.doi.org/10.1083/jcb.200508044

Rüegg, M.A., and D.J. Glass. 2011. Molecular mechanisms and treatment options for muscle wasting diseases. *Annu. Rev. Pharmacol. Toxicol.* 51:373–395. http://dx.doi.org/10.1146/annurev-pharmtox-010510-100537

Sato, A., H. Yamamoto, H. Sakane, H. Koyama, and A. Kikuchi. 2010. Wnt5a regulates distinct signalling pathways by binding to Frizzled2. *EMBO J.* 29:41–54. http://dx.doi.org/10.1038/emboj.2009.322

Schlegel, R., R.B. Dickson, M.C. Willingham, and I.H. Pastan. 1982. Amantadine and dansylcadaverine inhibit vesicular stomatitis virus uptake and receptor-mediated endocytosis of alpha 2-macroglobulin. *Proc. Natl. Acad. Sci. USA*. 79:2291–2295. http://dx.doi.org/10.1073/pnas.79.7.2291

Seale, P., L.A. Sabourin, A. Girgis-Gabardo, A. Mansouri, P. Gruss, and M.A. Rudnicki. 2000. Pax7 is required for the specification of myogenic satellite cells. *Cell*. 102:777–786. http://dx.doi.org/10.1016/S0092-8674(00)00066-0

Seifert, J.R., and M. Mlodzik. 2007. Frizzled/PCP signalling: a conserved mechanism regulating cell polarity and directed motility. *Nat. Rev. Genet.* 8:126–138. http://dx.doi.org/10.1038/nrg2042

Siegel, A.L., K. Atchison, K.E. Fisher, G.E. Davis, and D.D. Cornelison. 2009. 3D timelapse analysis of muscle satellite cell motility. *Stem Cells*. 27:2527–2538. http://dx.doi.org/10.1002/stem.178

Skuk, D., M. Paradis, M. Goulet, and J.P. Tremblay. 2007. Ischemic central necrosis in pockets of transplanted myoblasts in nonhuman primates: implications for cell-transplantation strategies. *Transplantation*. 84:1307–1315. http://dx.doi.org/10.1097/01.tp.0000288322.94252.22

Soleimani, V.D., V.G. Punch, Y. Kawabe, A.E. Jones, G.A. Palidwor, C.J. Porter, J.W. Cross, J.J. Carvajal, C.E. Kockx, W.F. van IJcken, et al. 2012. Transcriptional dominance of Pax7 in adult myogenesis is due to high-affinity recognition of homeodomain motifs. *Dev. Cell*. 22:1208–1220. http://dx.doi.org/10.1016/j.devcel.2012.03.014

Subauste, M.C., M. Von Herrath, V. Benard, C.E. Chamberlain, T.H. Chuang, K. Chu, G.M. Bokoch, and K.M. Hahn. 2000. Rho family proteins modulate rapid apoptosis induced by cytotoxic T lymphocytes and Fas. *J. Biol. Chem.* 275:9725–9733. http://dx.doi.org/10.1074/jbc.275.13.9725

von Maltzahn, J., C.F. Bentzinger, and M.A. Rudnicki. 2011. Wnt7a-Fzd7 signalling directly activates the Akt/mTOR anabolic growth pathway in skeletal muscle. *Nat. Cell Biol.* 14:186–191. http://dx.doi.org/10.1038/ncb2404

von Maltzahn, J., J.M. Renaud, G. Parise, and M.A. Rudnicki. 2012. Wnt7a treatment ameliorates muscular dystrophy. *Proc. Natl. Acad. Sci. USA*. 109:20614–20619. http://dx.doi.org/10.1073/pnas.1215765109

von Maltzahn, J., A.E. Jones, R.J. Parks, and M.A. Rudnicki. 2013a. Pax7 is critical for the normal function of satellite cells in adult skeletal muscle. *Proc. Natl. Acad. Sci. USA*. 110:16474–16479. http://dx.doi.org/10.1073/pnas.1307680110

von Maltzahn, J., R. Zinoviev, N.C. Chang, C.F. Bentzinger, and M.A. Rudnicki. 2013b. A truncated Wnt7a retains full biological activity in skeletal muscle. *Nat Commun*. 4:2869. http://dx.doi.org/10.1038/ncomms3869

Wang, Y.X., and M.A. Rudnicki. 2012. Satellite cells, the engines of muscle repair. *Nat. Rev. Mol. Cell Biol.* 13:127–133.

Wang, Y.X., C.F. Bentzinger, and M.A. Rudnicki. 2013. Treating muscular dystrophy by stimulating intrinsic repair. *Regen. Med.* 8:237–240. http://dx.doi.org/10.2217/rme.13.27

Willert, K., and R. Nusse. 2012. Wnt proteins. *Cold Spring Harb. Perspect. Biol.* 4:a007864. http://dx.doi.org/10.1101/cshperspect.a007864

Wu, X., X. Tu, K.S. Joeng, M.J. Hilton, D.A. Williams, and F. Long. 2008. Rac1 activation controls nuclear localization of beta-catenin during canonical Wnt signaling. *Cell*. 133:340–353. http://dx.doi.org/10.1016/j.cell.2008.01.052

Yin, H., A. Pasut, V.D. Soleimani, C.F. Bentzinger, G. Antoun, S. Thorn, P. Seale, P. Fernando, W. van Ijcken, F. Grosveld, et al. 2013a. MicroRNA-133 controls brown adipose determination in skeletal muscle satellite cells by targeting Prdm16. *Cell Metab.* 17:210–224. http://dx.doi.org/10.1016/j.cmet.2013.01.004

Yin, H., F. Price, and M.A. Rudnicki. 2013b. Satellite cells and the muscle stem cell niche. *Physiol. Rev.* 93:23–67. http://dx.doi.org/10.1152/physrev.00043.2011

Yu, A., J.F. Rual, K. Tamai, Y. Harada, M. Vidal, X. He, and T. Kirchhausen. 2007. Association of Dishevelled with the clathrin AP-2 adaptor is required for Frizzled endocytosis and planar cell polarity signaling. *Dev. Cell*. 12:129–141. http://dx.doi.org/10.1016/j.devcel.2006.10.015

Yu, H., X. Ye, N. Guo, and J. Nathans. 2012. Frizzled 2 and frizzled 7 function redundantly in convergent extension and closure of the ventricular septum and palate: evidence for a network of interacting genes. *Development*. 139:4383–4394. http://dx.doi.org/10.1242/dev.083352